Beam-Dynamics Studies and Advanced Accelerator Research at CTF-3: Compact Final Focus, Laser Compton Scattering, Plasmas, etc.

R. Assmann, H. Braun, H. Burkhardt, R. Corsini, S. Redaelli, D. Schulte, F. Zimmermann,
CERN, Geneva, Switzerland; A. Faus-Golfe, IFIC, Valencia, Spain;
M. Velasco, Northwestern University, IL, USA; J. Gronberg, LLNL Livermore, USA

Abstract

Preliminary investigations are summarized on the possible use of the CTF3 facility for extended beam-dynamics studies and advanced accelerator R&D, which would exploit its unique properties and beam availability. The key element of these considerations is the possible addition of a test beam-delivery system comprising a compact final focus and advanced collimation concepts, scaled from 3 TeV down to low energy and having a short total length. Operational experience, verification of critical questions (octupole tail folding, beam halo transport, etc.), diagnostics (*e.g.*, rf BPMs) and stabilization could all be explored in such a facility, which would benefit not only the CLIC study, but all linear collider projects. Another interesting application would be the study of plasma-beam interaction, which may include plasma focusing, plasma acceleration, ion-channel radiation, and plasma wigglers.

1 INTRODUCTION

In the context of the Nanobeam 2002 workshop, discussions started on the use of CTF-3 beyond present goals of drive-beam generation and 30-GHz rf power tests [1]. A first brainstorming gave a long list of possible study items (we here give only the keywords):

- Final-focus test stand. Construct a 10–20 m long Raimondi final focus [2] for a first experimental demonstration of such a system, at a beam energy of 150–400 MeV; produce 100–500 nm size beams in this facility; test precision diagnostics (conventional and rf BPMs with 10s of nm resolution, profile monitors); demonstrate active stabilization for an operating beam line and detect the effect on the beam motion; octupole tail folding; nonlinear collimation system; halo generation and transport; collimation and wake fields; measure the combined effect of crab cavities, crossing angle, and (weak) 'detector' solenoid on the vertical spot size at the focal point; photon-collider testbed, which can demonstrate beam-based stabilization of the laser system and multiple laser-beam collisions.

- Diagnostics. Develop and test multibunch BPMs and rf BPMs; use rf BPMs to measure the trajectory slope and bunch tilt; bunch length and beam profile measurements.

- Wake Fields. Measure multibunch wake fields in the linac, and wake fields from collimators.

- Feedback. Test of linac orbit feedback for CLIC beam structure. Test of fast inter-bunch train feedbacks. Demonstration of CLIC beam loading compensation.

- X-ray source. RF wiggler or Compton scattering using a laser. (These could be interesting options for the damping ring.)

- Advanced ideas, high-gradient studies, and plasma applications. Two final foci with collisions; beam splitting using rf deflectors; recirculation and energy recovery studies; beam-beam compensation; plasma acceleration; plasma wiggler (also of interest for the damping ring); plasma lens; plasma gun.

- Others. Positron target test; radiation physics; polarized positron source. Flat-beam photo-rf gun. DC gun à la Shintake.

Most intriguing seems to be the construction of a compact final focus, which is not only of interest in itself, but at the same time could provide the beam and the location for (almost) all the other studies mentioned. The final focus must be scaled from the 3-TeV design to low energy (and large emittance). As we shall show below, the final focus could produce spot sizes of a few 100 nm; it should readily allow for an experimental verification of beam-halo transport, tail folding using octupoles, and nonlinear collimation.

Two test facilities containing a similar compact final focus system are under consideration at SLAC and KEK. The SPHINX/LINX facility was proposed at the former SLC/SLD in Stanford [3]. The proposal includes a testbed for photon collider R&D. An upgrade comprising a compact final focus was also studied for the KEK/ATF [4]. The beam energy in both these alternative facilites would be higher than what can be realized at CTF-3, namely about 30 GeV for LINX and 1.3 GeV at the ATF. In addition, the ATF final focus would have the advantage of using a low-emittance beam extracted from the damping ring. On the other hand, the realization of either of these two projects is doubtful in view of funding difficulties and the high cost. The less expensive CTF-3 extension would offer the advantage of the potential operation with a multi-bunch train with a beam time structure similar to those foreseen in the CLIC and NLC designs, and a higher repetition rate than the ATF.

2 PARAMETERS AND SCHEDULE

Beam parameters for CTF-3 are listed in Table 1. The numbers refer to a single drive-beam bunch. The emittance val-

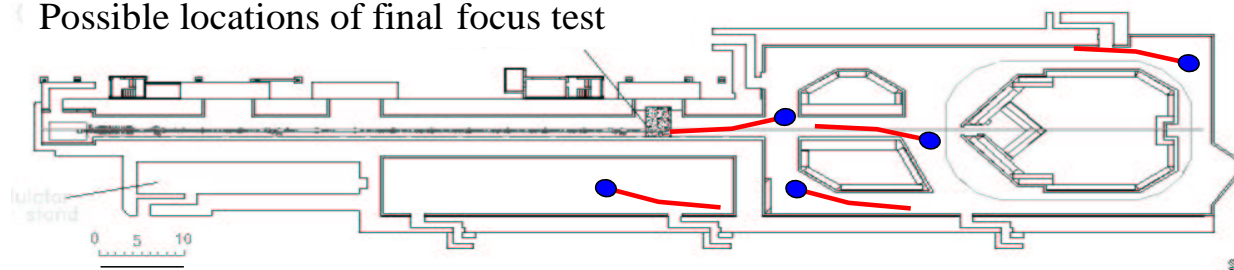Possible locations of final focus test

Figure 1: Footprint of CTF3, highlighting possible locations of the final-focus test stand.

ues assume that the beam is generated by an rf gun. A footprint of CTF-3 is shown in Fig. 1. Possible final-focus locations are indicated.

The CTF-3 time schedule is as follows. From 2003 to 2004 the drive beam linac will be constructed and commissioned. The delay loop will be put in place in 2005 and the combiner ring in 2006. A 200 MeV low charge probe-beam linac and an experimental area for two beam acceleration will be added once the drive beam generation complex is completed. In mid 2003 a decision will be taken on the construction of an RF photo-injector for the drive beam linac. If this decision is positive a beam with parameters as indicated in table 1 would be available from beginning of 2005. A compact final focus test could therefore be envisaged either in a location in the ring hall from 2005 on or later in the two beam acceleration test area (bottom left in the figure).

Table 1: Beam parameters

parameter	symbol	value
energy	E	200–400 MeV
emittance	$\gamma\epsilon_\perp$	1–4 μm
bunch length	σ_z	300 μm
momentum spread	σ_δ	0.1–0.35%
bunch population	N_b	$6 - 30 \times 10^9$
repetition rate	$f_{\rm rep}$	5 Hz
rf repetition rate	$f_{\rm rf,rep}$	30 Hz
bunch spacing	$L_{\rm sep}/c$	0.067–0.67 ns
no. bunches per pulse	n_b	1–2100

3   COMPACT FINAL FOCUS

A compact final focus has first been proposed by P. Raimondi and A. Seryi for the NLC [2]. Following the approach by S. Kuroda for the KEK ATF-II [4, 5], presented at Nanobeam 2002, shortly after the workshop we developed a design procedure for CTF-3, the details of which are discussed in Appendix A. A preliminary draft optics for CTF-3 parameters constructed by this procedure is shown in Fig. 2. The variation of the vertical and horizontal rms spot sizes with the vertical IP beta function is illustrated in

Figs. 3 and 4, for two different values of the rms energy spread, and a normalized emittance of 1 μm. Figures 5 and 6 show the dependence of the spot sizes on the normalized transverse emittances, varied simultaneously in both planes. Figures 7 and 8 display analogous results obtained by varying only one of the two transverse emittances at a time and keeping the other constant. The dependence of the spot sizes on the rms momentum spread is presented in Figs. 9 and 10. The geometrical footprint of the final focus is depicted in Fig. 11.
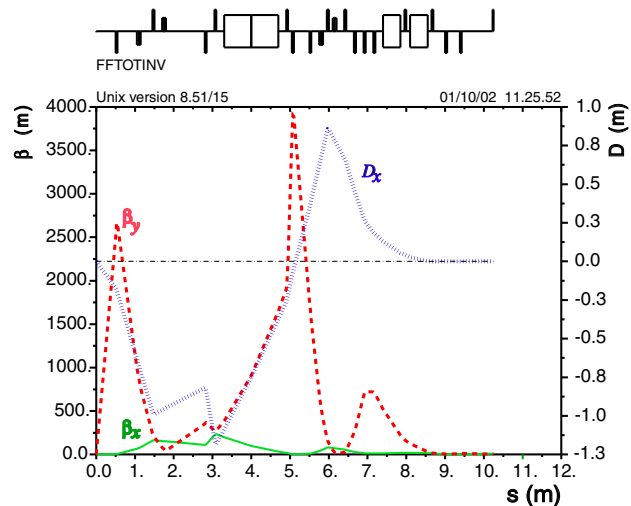

Figure 2: Draft optics for a compact final focus in CTF-3; beta functions for $\beta_x^* = 50$ mm, and $\beta_y^* = 0.1$ mm; dispersion for $D'^* = 0.346$ rad. The IP is on the left.

The parameters at the focal point are summarized in Table 2. For emittances less than 1 μm and a maximum energy spread of 0.2%, the vertical spot size varies between 200 nm and 1.5 μm. It appears that, for this draft system, a 500-nm spot size would be a reasonable experimental goal. The normalized emittance of about 1 μm requires a low-emittance photo-injector as the drive beam source for CTF-3. For an rms momentum spread below 0.1%, the horizontal beam size is a factor 4–6 larger than the value of 4–8 μm expected from the linear optics. The discrepancy increases
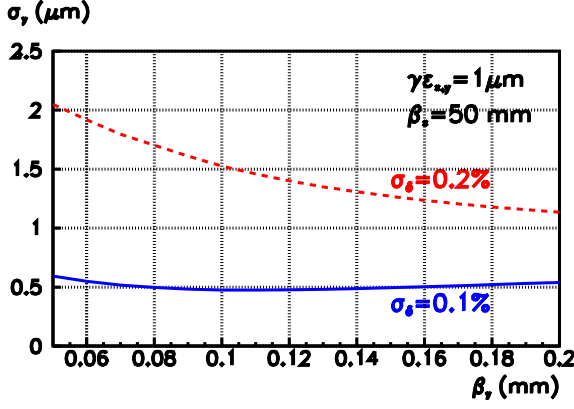
2

Figure 3: Vertical rms spot size vs. vertical beta function at focal point, for two different values of the rms momentum spread (0.1 and 0.2%), $\beta_x^* = 50$ mm, and $\gamma\epsilon_{x,y} = 1$ μm.

Figure 5: Vertical rms spot size at focal point vs. normalized transverse emittance ($\gamma\epsilon_x = \gamma\epsilon_y$), for two different values of the rms momentum spread (0.1 and 0.2%), $\beta_x^* = 50$ mm, and $\beta_y^* = 100$ μm.
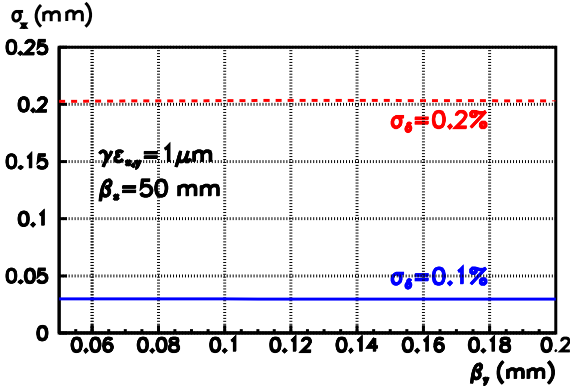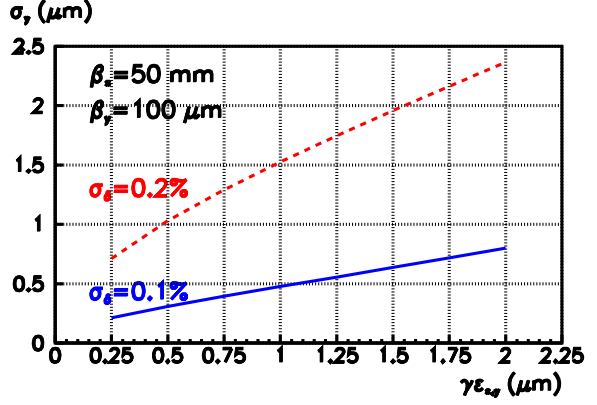

Figure 4: Horizontal rms spot size vs. vertical beta function at focal point, for two different values of the rms momentum spread (0.1 and 0.2%), $\beta_x^* = 50$ mm, and $\gamma\epsilon_{x,y} = 1$ μm.
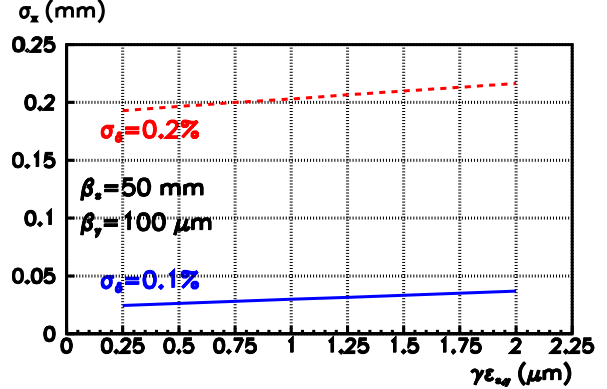

Figure 6: Horizontal rms spot size at focal point vs. normalized transverse emittance ($\gamma\epsilon_x = \gamma\epsilon_y$), for two different values of the rms momentum spread (0.1 and 0.2%), $\beta_x^* = 50$ mm, and $\beta_y^* = 100$ μm.

for larger momentum spreads. The horizontal spot size is completely dominated by dispersive and chromatic aberrations, since we have made no attempt to correct aberrations in the horizontal plane. In future studies, we may consider zeroing the 3rd order aberration for the horizontal plane by fulfilling Eq. (21) of Appendix A. Both horizontal and vertical beam sizes are very sensitive to the rms momentum spread. For example, doubling the momentum spread from 0.1% to 0.2% increases the vertical or horizontal spot size by factors of 3 or 6–7, respectively.

4 BEAM HALO STUDIES

Substantial beam halos were observed in the SLC. The origin was not identified. Beam halo collimation at high energies is expected to be difficult. It would be very useful to learn more about the origin of beam halos in linear accelerators and ways to minimize them. We propose to consider

to instrument the end of the linac or final focus sections for such studies.

Beam halo studies by tail scans using movable scrapers and beam loss monitors were pioneered in LEP [7]. They allowed quantitative beam halo studies over broad ranges of beam intensities and halo levels. We propose to consider to equip the final focus test with scrapers and loss monitors similar to what has been used in LEP. The aim of these studies would be to gain insight into the generation of beam halo at low energies and to validate existing modelling tools for the particle transport at large amplitudes. On the other hand, shower development and the number of secondaries produced by scraping are of less interest in this facility, since they will be quite different from those at multi-TeV energies.

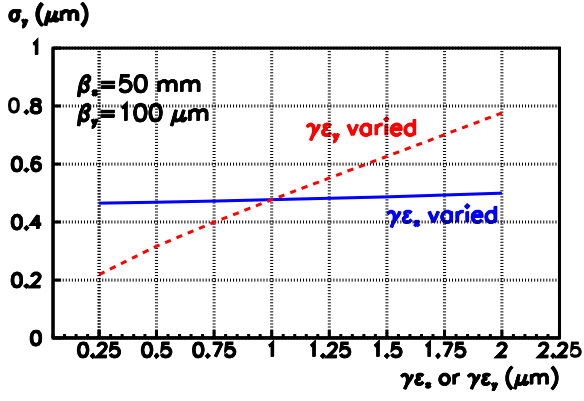Octupole tail folding at the final foublet was proposed

Figure 7: Vertical rms spot size at focal point vs. vertical or horizontal normalized emittance (the other emittance being kept constant at $\gamma\epsilon = 1$ μm), for an rms momentum spread of 0.1%, $\beta_x^* = 50$ mm, and $\beta_y^* = 100$ μm.

Figure 9: Vertical rms spot size at focal point vs. rms momentum spread for $\gamma\epsilon_{x,y} = 1$ μm, $\beta_x^* = 50$ mm, and $\beta_y^* = 100$ μm.
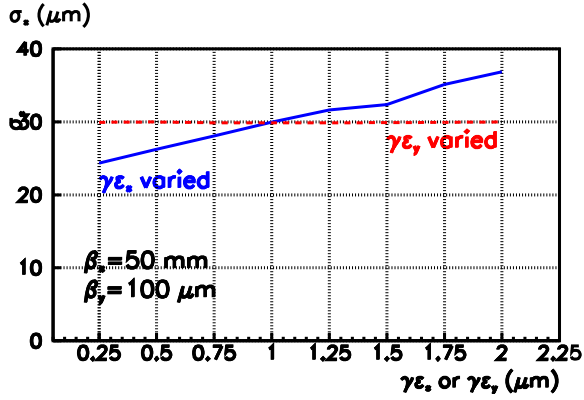

Figure 8: Horizontal rms spot size at focal point vs. vertical or horizontal normalized emittance (the other emittance being kept constant at $\gamma\epsilon = 1$ μm), for an rms momentum spread of 0.1%, $\beta_x^* = 50$ mm, and $\beta_y^* = 100$ μm.

Figure 10: Horizontal rms spot size at focal point vs. rms momentum spread for $\gamma\epsilon_{x,y} = 1$ μm, $\beta_x^* = 50$ mm, and $\beta_y^* = 100$ μm.

as a means to increase the required collimation depth and minimize wake-field effect [6]. This scheme has never been demonstrated experimentally for a linear-collider like beam, and there is some concern about the correct modelling of particle transport at large betatron amplitudes. A recent comparison of 4 codes revealed significant differences already at moderate amplitudes, and even in the absence of synchrotron radiation [8, 9]. That means that not only the generation of beam tails, but also their transport dynamics appears highly uncertain.

At Nanobeam 2002, the experimental demonstration of tail folding was considered to be necessary prior to construction of a next linear collider. The CTF-3 final focus test stand would allow for an experimental set up, whose results could be cross-checked with simulations.
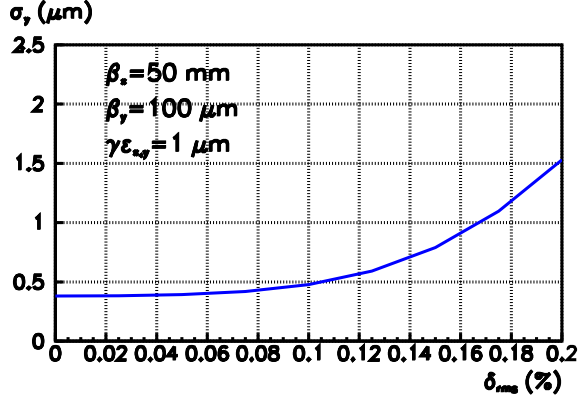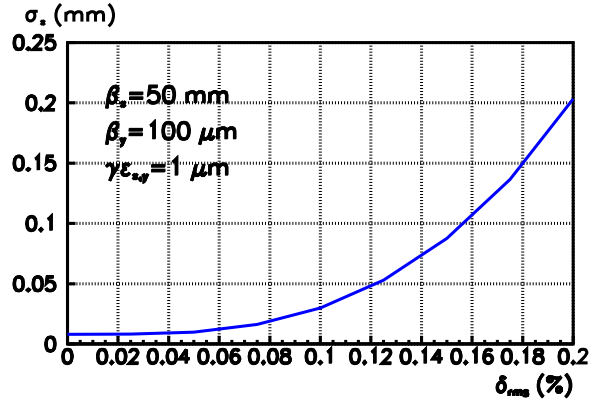
5 TUNING SCHEMES

Tuning the spot size (and luminosity) of a final focus is not a trivial task. At the SLC, the tuning procedures were improved every year, with large changes continuing even in the last months of operation. One of the goals of the FFTB at SLAC was to demonstrate the efficiency and convergence of the spot size tuning. While both the SLC and FFTB systems were modular systems, with obvious choices for the tuning knobs, this is no longer the case for the compact final-focus design. Here, the transfer matrices between a small number of quadrupoles are adjusted to comply with several constraints, and fulfill various functions at the same time.

One possibility for tuning is to vary the transverse positions of the sextupoles. Simulation studies for the NLC were reported in Ref. [10]. However, not every aberration can be corrected in this way. In particular the simultaneous correction of chromaticities and second order disper-
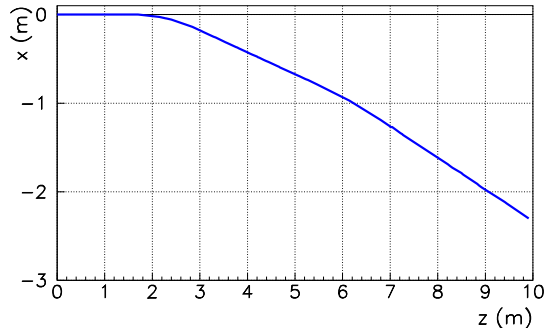
Figure 11: Footprint of the draft final focus, showing the horizontal displacement as a function of longitudinal position.

Table 2: Focal point parameters for draft optics. The values quoted for the vertical spot size assume an rms momentum spread of less than 0.2%, and a vertical normalized emittance below 1 μm. The numbers for the horizontal spot size either consider a horizontal normalized emittance smaller than 1 μm and an rms momentum spread of less than 0.1%, or, in the case of larger momentum spread, rely on a (partial) correction of the horizontal dispersive and chromo-geometric aberrations, which is still to be demonstrated.

variable	symbol	value
rms vertical beam size	σ_y^*	0.2–1.5 μm
rms horizontal beam size	σ_x^*	5–30 μm
vertical beta function	β_y^*	80–150 μm
horizontal beta function	β_x^*	10–50 mm

sion can pose problems, as will the higher-order terms.

A practical demonstration in CTF-3 will prove an invaluable method to learn more about the tuning potential of the compact final-focus system, and, if necessary, adapt the design according to the findings. A related issue is the identification of appropriate tuning signals.

Another interesting study would address a question raised by M. Ross at the workshop, namely whether and how tuning could be used to uncover the source of an error, which was barely done at the SLC.

6 FEEDBACK

Several feedbacks could be tested using BPM signals. Of interest is the performance of a fast intra-bunchtrain feedback (for the CLIC collision point), as well as a performance evaluation of linac orbit feedbacks for the CLIC main beam pattern and, possibly, the CLIC drive beam.

The CTF-3 bunch spacing prior to compression is 20 cm and, hence, it is identical to the spacing for the main beam in CLIC. The bunch spacing after compression is 2 cm, which is the same value as for the CLIC drive beam.

Therefore, CTF-3 would offer the unique opportunity to study and compare the performance of orbit feedbacks for all major parts of the CLIC project. Similar feedback studies are presently being conducted at the NLCTA for the NLC parameters, in the framework of the UK-funded FONT project [12].

Beam loading compensation is another issue of great importance and rather specific to CLIC.

7 COLLIMATION

For the 3-TeV CLIC, a nonlinear collimation system employing three skew sextupoles and a single vertical spoiler [11] have been investigated as an alternative to the traditional linear baseline system. A practical test of both linear and nonlinear collimation systems and a comparison of their respective performance would be desirable. This requires detectors, additional collimators, or sensitive profile diagnostics, which can detect and quantify the beam halo.

8 INSTRUMENTATION

If a test facility is built, the outcome will strongly depend on the available beam diagnostics. At least 10 precision BPMs are needed in the final focus alone, for optics monitoring and trajectory feedback.

8.1 Laser Wire, Profile diagnostics, and Bunch Length Measurements

Currently there is great interest in the possible use of a laser wire for non-destructive beam-size measurements in the 3-TeV CLIC beam-delivery system [13]. A prototype laser wire has been tested at CTF-2, where rather high background was observed [14]. If placed near the focal point of a CTF-3 test stand, a better resolution may be achieved. This might constitute one possibility for measuring and optimizing the small spot size. The laser Rayleigh length must be large compared with the horizontal beam size. Therefore, for applications using a laser wire it would be necessary either to reduce the horizontal spot size, or to measure larger vertical beam sizes, *e.g.*, away from the focal point. Namely, the laser wavelength required is [15]

$$\lambda \le \frac{4}{9}\pi\frac{\sigma_y^2}{\sigma_x} \, , \tag{1}$$

which is only 10 nm at the focal point for $\sigma_x \approx 30$ μm, and $\sigma_y \approx 500$ nm.

Other, perhaps more promising beam-size diagnostics include monitors using optical transition radiation or optical diffraction radiation [16].

Bunch length can be measured using rf signals picked up with an antenna, electro-optical monitors, or an rf streak (from rf deflector) as proposed for the LCLS project [17].

8.2 RF BPMS

Cavity BPMs are of great interest for a variety of reasons.

First, they can achieve an unparalleled resolution; 25 nm single-shot resolution was demonstrated at the FFTB. Placing three RF BPMs in series at the focal point would make it possible to identify the waist location and to infer the beta functions at the focal point. This might provide a much better and more reliable way to tune the final focus than a profile monitor, that is difficult to construct and potentially expensive.

Second, the signal from the RF BPM is sensitive to trajectory slope and to an internal tilt of the bunch [17].

Third, the evaluation and possible compensation of drifts in the position readings of both RF and regular BPMs would be an invaluable input to tuning and stability simulations.

Also novel electro-optical detectors could be developed and tested at the CTF-3 facility [17].

9   INTERACTION REGION

The combined effects of solenoid, crossing angle, crab cavities lead to an increase in the effective vertical spot size at the collision point, and to a significant reduction of luminosity. These effects might be reduced by a vertical crab cavity [18].

The experimental study of these effects (and possibly other related phenomena) and their correction at CTF-3 would be a valuable demonstration that no physics is missing and that the countermeasure functions as predicted. The solenoid could be very weak, *e.g.*, 100 G, should do. The 'virtual' crossing angle can be adjusted by rotating the solenoid. A horizontal rf deflector could serve as a crab cavity, and the compensation could be attempted via a second weaker and vertical rf deflector. A (time-resolved?) spot size measurement at the focal point would be desirable. Stabilization of the deflector rf phases with respect to the beam might also be looked at.

10   STABILIZATION & VIBRATION

The test stand would provide a unique extension of the extremely successful CLIC stability study [19]. By actively stabilizing real beam line elements, the direct effect on the beam motion could be studied, using BPMs. Roughly a third of the final focus, including the most critical components could be accommodated on the stabilized platform. There is no other comparable experiment planned anywhere in the world.

11   GAMMA-GAMMA R&D

Important aspects for the technical feasibility of a photon collider [20, 21, 22, 23] could also be tested at the CTF-3 final focus. For this purpose the SPHINX/LINX facility was proposed at the former SLC/SLD collision point in Stanford. However, the realization of this project appears doubtful due to budgetary reasons, and a less expensive alternative is called for. CTF-3 could suit this purpose. We propose to collide the single (drive) beam of CTF-3 with a single laser pulse to study several critical elements of the photon-photon scheme and its technology.

A prototype of the focusing mirrors along with their mounts, as designed for an LC interaction region would be installed. This would allow the stabilization of the laser focus relative to the beam to be demonstrated under realistic conditions. The mirror position would be varied by piezoelectric movers, in response to a signal from the laser-beam interaction, so as to optimize the beam-laser overlap and maintain an efficient conversion rate. Timing drifts between particle beam and laser are another issue which could be explored at this facility.

For a useful demonstration of stabilization the electron spot size must be smaller than the laser spot. The round laser spot size is of the order of 10 μm. The ideal spot size for the particle beam is also round. For this, the optics presented in Section 3 must be slightly modified. We expect that a spot size of 2–3 μm in both planes will be feasible at 400 MeV. Given the size of the laser, this spot appears sufficient.

A number of signals could be used to measure the conversion rate and provide a feedback signal to the stabilization. A small calorimeter could be used to directly measure the converted photons after the electron beam had been bent out of the way. Given that each conversion degrades the energy of one of the electrons in the bunch, another method would be to monitor the spent electron beam using a downstream energy spectrometer.

Unlike SLC, which runs with a single electron bunch, the multi-bunch capability of CTF-3 (at a lower energy of about 150 MeV) opens a new possibility for testing photon collider technology. The photon collider design assumes that a single large laser pulse is split into sub-pulses and time delayed to match the electron beam format with a system of optics. These optics will be difficult to align and may degrade the quality of the laser pulse. The CTF-3 facility would allow such a system to be prototyped and demonstrated.

The nominal CTF-3 repetition rate is 5 Hz, though the rf repetition rate is 30 Hz (which might suggest that one could also run beam at 30 Hz). The bunch-to-bunch spacing can be varied from 0.67 ns down to 0.067 ns, and there are 2100 bunches per pulse. By using every fifth pulse and running at 0.67 ns a bunch train very similar in time structure to the NLC beam could be simulated. The 0.67 ns corresponds to the nominal bunch spacing in CLIC.

12   WAKE FIELDS

Wake fields have been a concern throughout the life of the SLC. In particular, the verification of multi-bunch wake fields and collimator wake fields would be of interest. The wake deflects an off-center trajectory, which can be detected with downstream BPMs. This could be part of the collimation study.

13 INJECTOR UPGRADES

At the Fermilab A0 beam line, the possibility of a flat-beam rf gun was demonstrated; an emittance ratio of 40 was obtained [24] (about a factor 6 change in each plane). Here, the cathode is placed in a strong solenoid field, and the ensuing rotation, after exiting through the solenoid fringe, is taken out by three skew quadrupoles, in such a way as to make the beam flat. Application to CTF-3 might yield a normalized emittance of 6 μm horizontally and 0.2 μm vertically. We should then reach a spot size below 200 nm.

A high-voltage pulsed or dc thermionic gun, *e.g.*, as considered by T. Shintake for the SSCS project, is predicted to provide a factor 2–5 lower emittance even than a photoinjector [25]. This would be an alternative approach of reaching emittances well below 1 μm.

14 PLASMA POSSIBILITIES

Plasmas can be used to focus or to accelerate. They have potential applications for high-gradient acceleration [26] or as a plasma lens in linear colliders [28]. Another different application would be to tailor the synchrotron radiation emitted by electrons in a plasma-focusing channel [29], so as to obtain fast damping, similar to the effect of a highly efficient wiggler with extremely short period. The use of such 'plasma wigglers' [30] could revolutionize the damping ring design.

15 OUTLOOK

Most of these ideas are still premature, and their pursuit will require a more detailed design study. Nevertheless, these ideas are interesting, because a much larger community could be involved than with the CTF-3 base program alone. The studies proposed here are of interest to all linear collider projects and the whole accelerator physics community. Advanced accelerator research in Europe is underdeveloped and, contrary to the US, completely disconnected from the big accelerator laboratories. CERN would have the opportunity to assume a core role and guide the European or worldwide initiatives.

We also recall that a similar final focus project has been proposed for the KEK/ATF. In case the KEK project is funded, which appears highly uncertain at the time of this writing, we should not duplicate the Japanese studies, but concentrate on different non-overlapping topics. Advanced accelerator research is also pursued at the BNL/ATF, which we could take as an excellent example of what can be achieved with limited resources, but a lot of imagination and vision. The EPFL Lausanne, PSI or other light sources may well be interested in a partial collaboration on X-ray FEL R&D. Last but not least, the CTF-3 offers a unique opportunity to test the key components of a photon collider.

17 REFERENCES

[1] G. Geschonke, A. Ghigo (eds.), "CTF3 Design Report," CERN-PS-2002-008-RF, CTF3-NOTE-2002-047, LNF-2002-008-IR (2002).

[2] P. Raimondi, A. Seryi, "Novel Final Focus Design for Future Linear Colliders," Phys. Rev. Letters **86**, 17 (2000) p. 3779

[3] T. Markiewiz, "NLC Vibration Program and LINC," Nanobeam 2002, Lausanne, these proceedings (2002).

[4] J. Urakawa, "A Plan of ATF Final Focus Test Beam Line," Nanobeam 2002, Lausanne, these proceedings (2002).

[5] S. Kuroda, "Final Focus Test Optics for the ATF," presentation in KEK APPI seminar (2002).

[6] R. Brinkmann, P. Raimondi, A. Seryi "Halo Reduction by Means of Nonlinear Optical Elements in the NLC Final Focus System," PAC 2001, Chicago (2001).

[7] H. Burkhardt, I. Reichel, G. Roy, Transverse Beam Tails due to Inelastic Scattering,' PRST-AB 3, 091001 (2000).

[8] S. Redaelli, et al., "Comparison of Different Tracking Codes for Beam Delivery Systems of Linear Colliders," EPAC 2002 Paris, and CERN-SL-2002-033 (2002).

[9] S. Redaelli, et al., "Simulation Tools for Luminosity Performance," Nanobeam 2002, Lausanne, these proceedings (2002).

[10] Y. Nosochkov, et al., "Tuning Knobs for the NLC Final Focus," Proc. EPAC 2002, Paris, France (2002).

[11] A. Faus-Golfe, F. Zimmermann, "A Nonlinear Collimation System for CLIC," 8th EPAC, Paris, France, 3 - 7 Jun 2002, and CERN-SL-2002-032 (2002).

[12] G. White, P. Burrows, et al., "Beam Dynamics Simulations, Banana Bunches, and IP Feedback Systems," Nanobeam 2002.

[13] G. Penn, "Simulation of Laser Wire in BDS," Nanobeam 2002.

[14] T. Levefre, "Laser Wire Scanner Test on CTF-2," Nanobeam 2002.

[15] J. Frisch, "Technical Challenges Outstanding," Nanobeam 2002, Lausanne, these proceedings (2002).

[16] J. Urakawa, "ATF Results," Nanobeam 2002, Lausanne, these proceedings (2002).

[17] M. Ross, "Instrumentation Development — Test Facilities and Plans," Nanobeam 2002, Lausanne, these proceedings (2002).

[18] M. Aleksa, et al., "CLIC Beam Delivery System," these proceedings.

[19] R. Assmann, et al., "Results of the CLIC Stability Study," these proceedings.

[20] V.I. Telnov, "Problems of Obtaining Gamma Gamma and Gamma Epsilon Colising Beams at Lineat Colliders," Nucl. Instrum. Meth. A294 (1990) 72

[21] H. Burkhardt, V. Telnov, "CLIC 3-TeV Photon Collider Option," CERN-SL-2002-013-AP, CLIC-NOTE-508 (2002).

[22] D. Asner et al, "Higgs Physics with a Gamma Gamma Collider BAsed on CLIC I," BNL-HET-01-32, CERN-PS-NOTE-2001-062-AE, CERN-SL-2001-055-AP, CERN-TH-2001-235, CLIC-NOTE-500, NUHEP-EXP-01-050, UCRL-JC-145692 (2001)

[23] M. Velasco, "Gamma-Gamma IR Issues," and "A Proposal to Demonstrate Gamma-Gamma Collisions at the SLC IP," Nanobeam 2002, Lausanne, these proceedings (2002).

[24] K.J. Kim, "Small Emittance Generation: Flat Beams," Nanobeam 2002, Lausanne, these proceedings (2002).

[25] L. Rivkin, "Linear Colliders and Light Sources: Issues of Common Interest," Nanobeam 2002, Lausanne, these proceedings (2002).

[26] M.J. Hogan, et al., "E-157: A 1.4 Meter Long Plasma Wake Field Acceleration Experiment using a 30-GeV Electron Beam from the Stanford Linear Accelerator Center Linac,' Phys. Plasmas 7, p. 2241 (2000).

[27] R. Assmann, "Review of Ultrahigh Gradient Acceleration Schemes, Results of Experiments," EPAC 2002, Paris (2002).

[28] J.S.T. Ng, "Observation of Plasma Focusing of a 28.5-GeV Positron Beam," Phys. Rev. Lett 87, 244801 (2001).

[29] E. Esarey, et al., "Synchrotron Radiation from Electron Beamcs in Plasma-Focusing Channels," Phys. Rev. E 65, 056505 (2002).

[30] S. Wang, et al., "X-Ray Emission from Betatron Motion in a Plasma Wiggler," Phys. Rev. Lett. 88, 135004 (2002).

[31] A. Seryi, Nanobeam 2002, September 2, 2002 (2002).

[32] J. Irwin, "The Application of Lie Algebra Techniques to Beam Transport Design," Nucl. Instrum. Meth. A298 (1990) 460

A FINAL-FOCUS DESIGN PROCEDURE

A.1 Recipe

The design recipe for the NLC compact final focus was outlined by A. Seryi at Nanobeam 2002 [31]. Here, we have followed an alternative design procedure which was inspired by S. Kuroda's scheme for ATF-II [4, 5]. It consists of the following steps:

(1) We first create a basic inverse beam line starting at the IP, consisting of 1 dipole, 8 quadrupoles (4 upstream and 4 downstream of the bending magnet), a specifically selected free length from IP to the first quadrupole, and 4 sextupoles, two upstream and to downstream of the dipole. The bending angle is set to a pre-selected value. Since synchrotron radiation is not an issue at 400 MeV (assumed maximum energy of a single bunch in CTF-3), we chose 50 mrad.

(2) We next match the two R matrices between conjugate pairs of sextupoles (1 + 3 and 2 + 4) to "pseudo" $-I$ transforms, with $R_{11} = R_{33}$, $R_{12} = R_{34} = 0$, but in general $R_{43} \neq 0$ and $R_{21} \neq 0$.

(3) We then adjust the strength of the final quadrupole, so as to minimize the quadratic sum of the 3rd order optical

aberrations U_{1244} (equal U_{3224}) and U_{3444}, computed as in Kuroda's paper. The final value of their quadratic sum is 10^{-3}, down from an initial value of 0.5. We discuss this constraint below.

(4) We launch the dispersion at the focal point with a nonzero slope such that the divergence due to the dispersion and energy spread is about equal to that from the horizontal emittance and beta function. We further add an upstream bending magnet and four quadrupoles, which are located between this bending magnet and the first sextupole. Still considering the inverse system (starting from the IP), we match the dispersion by adjusting the strengths of the 4 quadrupoles as well as the bending angle of the newly added dipole.

(5) Afterwards, we match the beta and alpha functions at the exit of the inverse system, or at the entrance of the real beam line, by adjusting the strengths of 4 quadrupoles which we introduce upstream of the first bend. The final focus is now (almost) complete, and its total length determined.

(6) We next invert this final-focus system and follow the direction of the beam propagation. In the simulation, we add the inverse of the total 4×4 R matrix at the entrance of the beam line, such that the 4×4 R matrix for the combined system is equal to the identity. We relate the strengths of the paired sextupoles (1 and 3, or 2 and 4) by $K_1 = -K_3 R_{11}^{13^3}$ and $K_2 = -K_4 R_{11}^{24^3}$, respectively, where R_{11}^{12} or R_{11}^{34} are the (1,1) matrix elements between sextupole 1 and 3 or 2 and 4. We then minimize the third order terms T_{166}, T_{126}, and T_{346}, by optimizing the strength of the two families of sextupoles.

(7) Since there are 3 constraints, and only two sextupole strengths, the last step does not fully converge. Therefore, we insert an additional quadrupole at the center of the first bend, and vary its strength. For each value of the quadrupole strength, we repeat the steps (4) to (6), until the values of T_{166}, T_{126}, and T_{346} are sufficiently small.

The system so obtained is fully corrected in 2nd and 3rd order. However, for the large emittances of CTF3, higher order aberrations limit the performance. These are not easily accessible in MAD.

A.2 3rd Order Aberrations

The primary aberrations arise from the 4 sextupoles. We analyse the combined system using the Lie algebra technique described by J. Irwin [32].

In a thin-lens approximation, the nonlinear Lie generators (acting on the IP coordinates) can be written as

$$\exp\left(-\frac{K_1}{6}(x_1^3 - 3x_1 y_1^2)\right) \exp\left(-\frac{K_2}{6}(x_2^3 - 3x_2 y_2^2)\right)$$
$$\exp\left(-\frac{K_3}{6}(x_3^3 - 3x_3 y_3^2)\right) \exp\left(-\frac{K_4}{6}(x_4^3 - 3x_4 y_4^2)\right) , \quad (2)$$

where the subindex 1, e.g., refers to the first sextupole in the beam line. Because of the pseudo $-I$ transformation,

we further have

$$x_3 = R_{11}^{13} x_1 \tag{3}$$
$$x_4 = R_{11}^{23} x_2 \ , \tag{4}$$

where for simplciity we omitted some additive terms related to dispersion, which would be of the form $R_{16}\delta$. Next, choosing the sextupole strengths as

$$K_1 = -K_3 R_{11}^{13\,3} \tag{5}$$
$$K_2 = -K_2 R_{11}^{24\,3} \ , \tag{6}$$

Eq. (2) simplifies to

$$\exp\left(\frac{K_3}{6}(x_3^3 - 3x_3 y_3^2)\right) \exp\left(\frac{K_4}{6}(x_4^3 - 3x_4 y_4^2)\right)$$
$$\exp\left(-\frac{K_3}{6}(x_3^3 - 3x_3 y_3^2)\right) \exp\left(-\frac{K_4}{6}(x_4^3 - 3x_4 y_4^2)\right) \ . \tag{7}$$

We recognize the familiar form of a similarity transformation, which allows us to re-express Eq. (7) as

$$\exp\left(\exp\left(\frac{K_3}{6}(x_3^3 - 3x_3 y_3^2)\right)\frac{K_4}{6}(x_4^3 - 3x_4 y_4^2)\right)$$
$$\exp\left(-\frac{K_4}{6}(x_4^3 - 3x_4 y_4^2)\right) \ . \tag{8}$$

The term on the far right-hand side would only contribute, via the CBH theorem, to higher-order aberrations which are proportional to the product of at least three sextupole strengths. We may ignore it here. Then, the 3rd order optical aberrations derive from the Hamiltonian of the left-hand term:

$$H_{\text{tot}} \approx -\exp\left(\frac{K_3}{6}(x_3^3 - 3x_3 y_3^2)\right)\frac{K_4}{6}(x_4^3 - 3x_4 y_4^2) \ . \tag{9}$$

Application of the Poisson brackets yields

$$[x_3^3, x_4] = 3x_3^2 Q_{12} \tag{10}$$
$$[-3x_3 y_3^2, x_4] = -3y_3^2 Q_{12} \tag{11}$$
$$[-3x_3 y_3^2, y_4] = -6x_3 y_3 Q_{34} \ , \tag{12}$$

where Q is the R matrix between the 3rd and 4th sextupole. We can, thus, expand the Hamiltonian (9) as

$$H_{\text{tot}} \approx -\frac{K_4}{6}\left[\left(x_4 + \frac{K_3}{2}(x_3^2 - y_3^2)Q_{12}\right)^3\right.$$
$$-3\left(x_4 + \frac{K_3}{2}(x_3^2 - y_3^2)Q_{12}\right)$$
$$\left.(y_4 - K_3 x_3 y_3 Q_{34})^2\right]$$
$$-\frac{K_4}{6}(x_4^3 - 3x_4 y_4^2)$$
$$\approx -\frac{K_4 K_3}{4}\left[x_4^2(x_3^2 - y_3^2)Q_{12}\right.$$
$$\left.-(x_3^2 - y_3^2)y_4^2 Q_{12} + 4x_4 x_3 y_3 y_4 Q_{34}\right] \ . \tag{13}$$

Adopting Kuroda's convention, and denoting the R matrix between the 4th sextupole and the IP by N, we can express the coordinates x_4, y_4, x_3, and y_3 in terms of those at the IP (subindex 0) as:

$$x_4 \approx -N_{12} x_0' \tag{14}$$
$$y_4 \approx -N_{34} y_0' \tag{15}$$
$$x_3 \approx -(N_{11}Q_{12} + N_{12}Q_{22})x_0' \tag{16}$$
$$y_3 \approx -(N_{33}Q_{34} + N_{34}Q_{44})y_0' \ , \tag{17}$$

where, as before, we do not include dispersive terms. Inserting these relations into Eq. (13) we obtain the coefficients of the higher-order generators:

$$H_{\text{tot}} \approx -\frac{K_4 K_3}{4}\left[Q_{12}N_{34}^2(N_{33}Q_{34} + N_{34}Q_{44})^2 y_0'^4\right.$$
$$+ \left\{-Q_{12}N_{12}^2(N_{33}Q_{34} + N_{34}Q_{44})^2\right.$$
$$-Q_{12}N_{34}^2(N_{11}Q_{12} + N_{12}Q_{22})^2$$
$$+4Q_{34}N_{12}N_{34}(N_{33}Q_{34} + N_{34}Q_{44})$$
$$(N_{11}Q_{12} + N_{12}Q_{22})\} x_0'^2 y_0'^2$$
$$\left.+ \left(Q_{12}N_{12}^2(N_{11}Q_{12} + N_{12}Q_{22})^2\right) x_0'^4\right] \tag{18}$$

We thereby recover the two matching conditions quoted by S. Kuroda (without derivation):

$$Q_{12}N_{34}^2(N_{33}Q_{34} + N_{34}Q_{44})^2 = 0 \tag{19}$$
$$-Q_{12}N_{12}^2(N_{33}Q_{34} + N_{34}Q_{44})^2$$
$$-Q_{12}N_{34}^2(N_{11}Q_{12} + N_{12}Q_{22})^2$$
$$+4Q_{34}N_{12}N_{34}(N_{33}Q_{34} + N_{34}Q_{44})$$
$$(N_{11}Q_{12} + N_{12}Q_{22}) = 0 \ . \tag{20}$$

In addition, we find the matching condition for the horizontal plane:

$$Q_{12}N_{12}^2(N_{11}Q_{12} + N_{12}Q_{22})^2 = 0 \ . \tag{21}$$

B MAGNET PARAMETERS FOR DRAFT FINAL FOCUS

Table 3 compiles parameters for all magnets in the draft final focus, including their length, strength, and the corresponding rms beam sizes, assuming pessimistic parameters (small values for the IP beta functions, and a large energy spread). From the rms beam size we can infer the minimum half apertures required, which may be about 10 rms beam sizes. The quadrupoles are up to 10 times stronger than typical CTF-3 magnets.

For this first draft optics design, rather arbitrarily very short quadrupoles were selected. which do not yet correspond to a 'technical' solution. The requirement on the high field gradient could be relaxed by increasing the length of the magnets, or, alternatively, the quadrupole gradients could be increased by building new magnets with smaller apertures, or modifying the poles of existing magnets accordingly. Another option might be to increase the length of the entire system by a factor 2 or 3, with an accompanying decrease in the quadrupole gradients.

Table 3: Magnet list for the draft CTF3-FF optics; quoted beam sizes assume $\beta_x^* = 20$ mm, $\beta_y^* = 0.08$ mm, $\gamma\epsilon_{x,y} = 1$ μm, $\delta_{\text{rms}} = 0.2\%$, $E = 400$ MeV.

name	type	position [m]	length [m]	angle [rad]	σ_x [mm]	σ_y [mm]
B1	SBEND	4.0000	1.4000	0.1000	0.5611	1.2035
B2	SBEND	7.8500	0.4500	0.2424	0.6022	0.5961
name	type	position [m]	length [m]	gradient [T/m]	σ_x [mm]	σ_y [mm]
Q1	QUADRUPOLE	0.5250	0.0500	-73.1608	0.1350	2.0634
Q2	QUADRUPOLE	1.4750	0.0500	26.8480	0.7195	0.5873
Q3	QUADRUPOLE	2.8250	0.0500	-53.1544	0.6025	0.7656
Q4	QUADRUPOLE	3.0750	0.0500	44.9415	0.8616	0.6562
Q5	QUADRUPOLE	4.9250	0.0500	69.2061	0.3035	1.7860
Q6	QUADRUPOLE	5.0750	0.0500	-78.5433	0.1809	2.4956
Q7	QUADRUPOLE	5.5250	0.0500	-8.2233	0.2923	1.6252
Q8	QUADRUPOLE	5.9750	0.0500	48.9609	0.6003	0.4974
Q9	QUADRUPOLE	6.4250	0.0500	15.4788	0.4499	0.2357
Q10	QUADRUPOLE	6.6750	0.0500	-5.3773	0.3126	0.6719
Q11	QUADRUPOLE	6.9250	0.0500	-41.5471	0.2191	1.0669
Q12	QUADRUPOLE	7.1750	0.0500	-16.9931	0.2688	1.0660
Q12B	QUADRUPOLE	7.9750	0.0500	11.1151	0.6469	0.5097
Q13	QUADRUPOLE	8.6750	0.0500	47.4362	0.6288	0.1665
Q14	QUADRUPOLE	9.0250	0.0500	-126.2903	0.2050	0.0933
Q15	QUADRUPOLE	9.4060	0.0500	-137.1997	0.0979	0.1401
name	type	position [m]	length [m]	sext. gradient [T/m^2]	σ_x [mm]	σ_y [mm]
S1	SEXTUPOLE	1.0999	0.1000	-1352.4841	0.4904	1.1817
S2	SEXTUPOLE	1.7500	0.1000	853.7906	0.6977	0.3069
S3	SEXTUPOLE	5.8000	0.1000	-2743.9461	0.4809	0.9335
S4	SEXTUPOLE	6.1500	0.1000	2689.7669	0.5446	0.2094